Experimental Investigation of Apex Fence Flaps on Delta Wings

Richard A. Wahls,* Robert J. Vess,† and Cary A. Moskovitz*
North Carolina State University, Raleigh, North Carolina

An exploratory wind tunnel investigation, involving pressure surveys and flow visualization, was performed to observe the flowfield effects produced by vertically deployed "apex fences" on a highly swept delta wing. The fence-generated vortices were intended to alter the upper-surface vortex patterns and associated induced pressures in such a way as to improve the lift and pitching moment characteristics of the planar delta. It was determined that relatively small apex fences, when symmetrically deployed, enhance the average suction level on the wing upper surface, which may amount to a 10% increase in the average pressure coefficient for angles of attack of 0–20 deg. Indications are that even higher suction levels may occur over the wing apex region between the fences, producing a nose-up pitching moment for longitudinal trimming (i.e., when trailing-edge flaps are used for lift increment).

Nomenclature

C_R = wing root chord, in.
$C_{p,u}$ = upper-surface pressure coefficient
$\Delta\overline{C}_{p,u}$ = average upper-surface pressure coefficient
$\Delta\overline{C}_{p,u}$ = upper-surface average pressure coefficient increment ($\Delta\overline{C}_{p,u} = \overline{C}_{p,u} - \overline{C}_{p,u,p}$)
t = wing thickness, in.
X = longitudinal coordinate, in.
α = angle of attack, deg
η = spanwise coordinate normalized by the local semispan
Λ = sweep angle, deg

Superscripts

f = fence
p = planar case

Introduction

In recent years, much research has been directed toward the development of supersonic cruise aircraft endowed with a high level of subsonic maneuverability. It is well known that the aerodynamics of the highly swept delta wing, which is frequently selected for supersonic aircraft due to its low wave drag characteristics, are largely determined by the formation and behavior of leading-edge vortices. Accordingly, the study of vortex characteristics has attracted renewed interest, particularly in the context of controlling and modifying them to the aerodynamicist's advantage. A variety of vortex management concepts have been proposed and investigated in recent years,[1] aimed at developing practical devices for specific aerodynamic functions such as lift augmentation, drag reduction, and flight path control.

Conceptually, the "apex fence" is an upper-surface hinged panel located in the apex region of the wing as shown in Fig. 1. It was originally proposed by Rao as a vortex control concept for delta wings or related planforms such as cranked and arrow wings. These wings have a highly swept apex region whose nonlinear aerodynamic characteristics, such as vortex-induced lift and pitching moment, could be modulated independently of the angle of attack. The fence flap is designed to lie flat on the wing upper surface during supersonic cruise so that no cruise drag penalty will occur. Like the upper vortex flap,[2] the apex fence is controlled by varying its upward deflection angle with respect to the wing plane. The apex fence is intended for functions similar to the apex flap,[3,4] although its geometry and vortex-generation characteristics have more in common with the upper vortex flap.[2]

This investigation involved tests of apex fences on two delta wing models. The initial testing was conducted on a 74 deg, full-span delta wing. Fence deflections were fixed at 90 deg. The tests included symmetrical as well as asymmetrical arrangements (i.e., with fences on both sides or one side only), the latter representing a lateral-directional control mode.

The second phase of the investigation was a study of fence geometry and location on a 65 deg, semispan delta wing. The effects of two fence shapes and four fence positions, all deflected 90 deg, were observed through flow visualizations and upper-surface pressure measurements.

Models

Model 1

A 74 deg, full-span, flat delta planform with a 20 in. root chord was constructed using a 0.375 in. thick balsa core with fiberglass/polyester resin facings (Fig. 1). In the interest of simplicity, the leading edges were beveled 45 deg only on the lower surface to provide a sharp leading edge and a definite separation point. Data presented by Rao and Buter[3,4] suggest that, although the leading edges experience a local negative camber effect which promotes premature separation, this geometry is perfectly acceptable since the present investigation involves direct comparisons with the planar wing.

Model 1 incorporated three spanwise rows of upper-surface static pressure taps located at $X/C_R = 0.50$, 0.65, and 0.80 with 11, 15, and 18 taps/row, respectively. All taps were located in the right semispan of the wing and extended from the centerline to approximately 90, 95, and 94% of the local semispan, respectively. One tap on the $X/C_R = 0.50$ row was found to be defective and is not presented in the results.

A pair of apex fences (Fig. 1) was cut from 0.125 in. thick plywood in the shape of right triangles, i.e., a semispan delta wing shape. The fence size was determined with two specifications in mind: 1) each would extend along the leading edge at $X/C_R = 0.0$–0.25; and 2) when folded onto the main wing, the leading edge of the fences would meet at the apex centerline.

Presented as Paper 85-4055 at the AIAA 3rd Applied Aerodynamics Conference, Colorado Springs, CO, Oct. 14-16, 1985; received Nov. 8, 1985; revision received May 30, 1986.

*Graduate Student in Aerospace Engineering. Student Member AIAA.
†Lecturer, Mechanical and Aerospace Engineering. Member AIAA.

These constraints provided a total fence area of approximately 6.75% of the total wing area. After beveling the leading edge of the fences, they were affixed perpendicularly to the wing leading edges.

Model 2

A 65 deg, semispan delta planform was used in the second phase of the investigation (Fig. 2). Whereas model 1 was mounted on a three-strut support system, model 2 was placed vertically in the wind tunnel on a reflection plate that raised it out of the boundary layer on the tunnel floor while still providing a solid plane of symmetry. This model was constructed from a foam core with plywood ribs and was sheeted, as before, with fiberglass. The wing had a 30 in. root chord and a maximum thickness ratio of $t/C_R = 0.0357$ and both upper and lower surfaces were beveled to provide a sharp leading edge. A row of 43 pressure taps was installed at $X/C_R = 0.70$ extending from $\eta = 0.049$ to 0.964.

Two types of apex fences were constructed for testing (Fig. 2). The first was a 74 deg, semispan delta shape similar to that used with model 1. Its area was approximately 4.91% of the

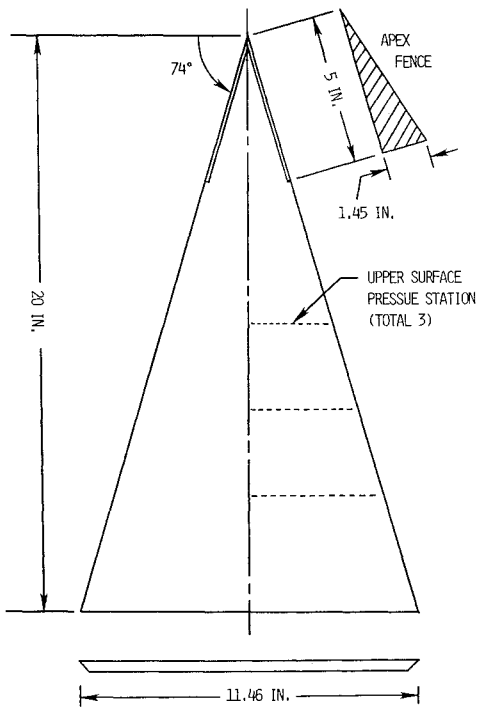

Fig. 1 Model of 74 deg delta wing.

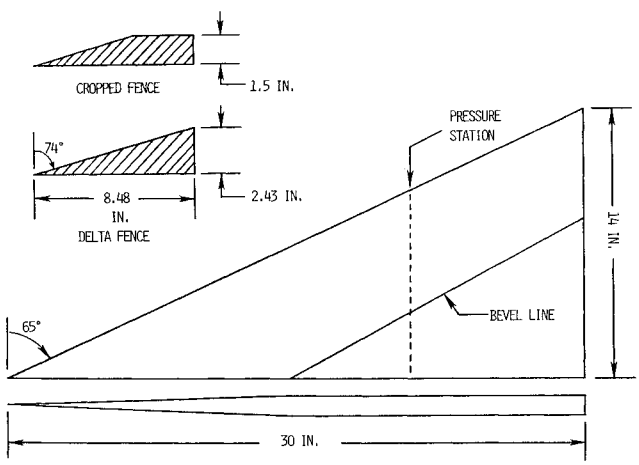

Fig. 2 Model of 65 deg semispan delta wing.

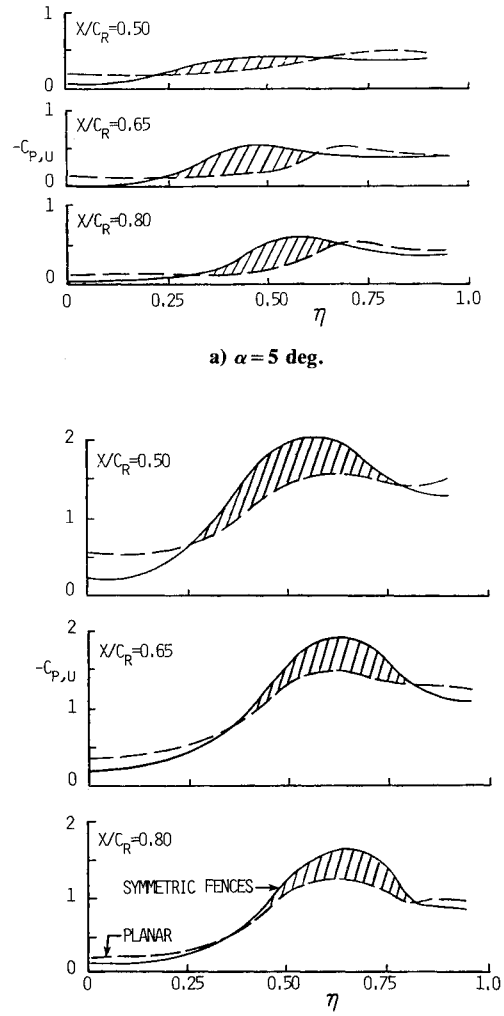

Fig. 3 Upper-surface pressure distribution.

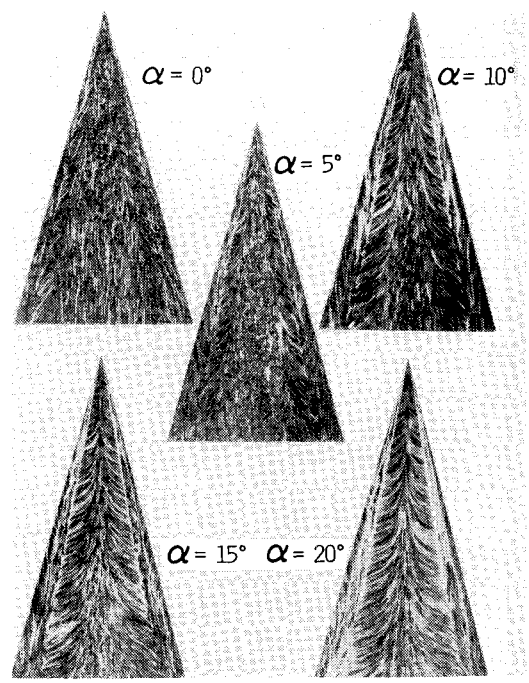

Fig. 4 Surface oil flow visualization, planar case.

main wing. The second was identical to the first with the exception of the cropped tip, which reduced its area to 4.19% that of the main wing. Each fence, along with a flange connected at the root, was cut from a sheet of 0.05 in. aluminum. The fences were then easily attached to one of four locations in the apex region. Again, the fences were tested only with a deflection perpendicular to the wing surface.

Both models were tested in the subsonic wind tunnel at North Carolina State University.

Experimental Technique

Pressure Tests

Pressure tests were conducted with a 48 channel pressure scanner that measured the static pressures on the upper surface of the models at a flow velocity of 60 mph. This corresponded to a Reynolds number of approximately 510,000/ft for each model. Pressure coefficients were obtained with an accuracy of ± 0.005 and were then averaged across the span at a specific chord location to generate the local average upper-surface pressure coefficient $\overline{C_{p,u}}$.

Flow Visualization

Two methods of flow visualization were employed. The first of these was the oil flow method that displays the surface flow pattern. Thirty-weight motor oil whitened with titanium dioxide was sprayed on the model such that small droplets covered the upper surface. The flow velocity was 60 mph, which corresponded, as in the pressure survey, to a Reynolds number of 510,000/ft. This method was used only with model 1.

The second method, which was applied to both models, involved using a bubble generator that used a combination of helium, soap, and air to form streams of neutrally buoyant bubbles. The bubble source was held sufficiently far upstream of the model in order to allow the bubbles to follow the natural path of the streamlines flowing over the model. These tests were conducted at 15 mph and a Reynolds number of approximately 127,500/ft. During the test of model 1, an arc lamp was placed downstream of the test section and illuminated the bubbles passing over the model, while avoiding glare on its surface. For model 2, a system of mirrors was placed downstream of the test section and the arc lamp was located outside the tunnel.

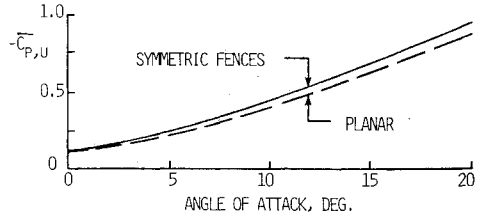

a) Upper-surface average pressure coefficient.

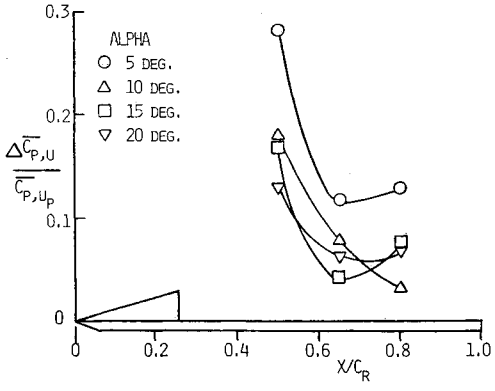

b) Local average pressure coefficient increment.

Fig. 5 Local average pressure coefficient distributions.

Results and Discussion

Model 1

Planar Wing

In order to evaluate the apex fence effects, it was necessary to first establish the planar wing characteristics. Although the aerodynamics of a planar, 74 deg delta wing are well known, the large asymmetric bevel on the leading edges of the model simulated a negative camber and was expected to influence the vortex growth characteristics and, consequently, the upper-surface pressure with increasing angle of attack. As expected, leading-edge separation was observed at $\alpha = 0$ deg. Representative pressure distributions for the planar wing, as well as the symmetric fence case, are presented in Fig. 3. Further documentation can be found in Refs. 5 and 6. The primary vortex developed normally, as indicated by the rising suction peak and its inboard movement with increasing angle of attack. The oil flow patterns in Fig. 4 clearly display this vortex development pattern.

Symmetric Apex Fences

As shown previously, a comparison of the upper-surface pressure distributions at the three chordwise stations is given in Fig. 3 for the wing with and without symmetrically deployed apex fences. Typically, the fences result in a suction peak located between $\eta = 0.50$ and 0.70, which is generally higher in magnitude than the planar wing suction peak. The boost in the maximum suction level (see shaded region) increases markedly with the angle of attack. On the other hand, the suction level both near the centerline and the leading edges is reduced, as is particularly evident at the forward station ($X/C_R = 0.50$). The local upper-surface average pressure coefficient, presented in Fig. 5, shows an increase in the presence of fences at all angles of attack except zero. In Fig. 5a, note that the average presented is one combining all three of the chordwise tap stations. The average increase in local $-\overline{C_{p,u}}$ is approximately 10% over a region comprising the aft 75% of the total wing area. There is also a strong trend of increasing local $-\overline{C_{p,u}}$ toward the forward station, implying an even higher value over the remaining portion forward of the root quarter chord.

The oil flow patterns with symmetric fences (Fig. 6) show, in each case, a vortex pair having a stronger "footprint" than evident at the same incidence on the planar wing, as judged by

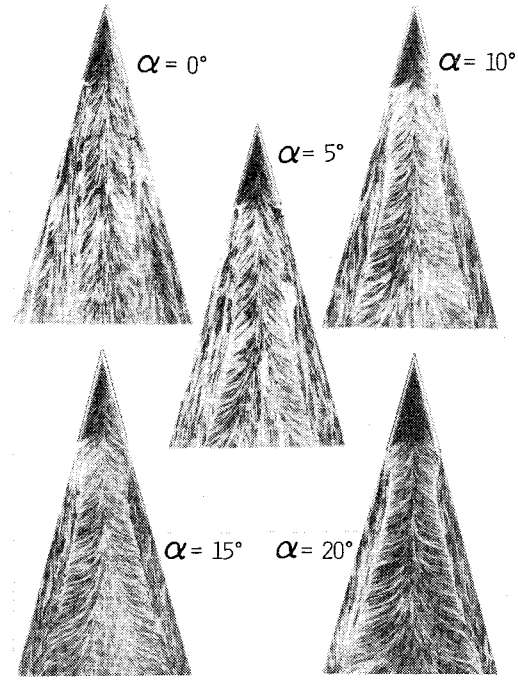

Fig. 6 Surface oil flow visualization, symmetric fences.

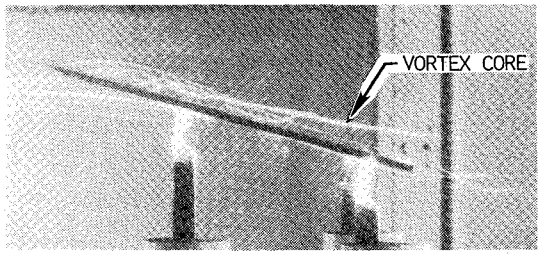

a) Planar, $\alpha = 15$ deg.

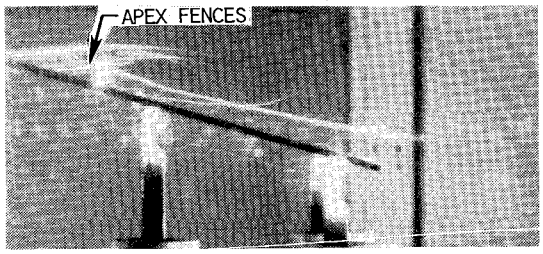

b) Symmetric fences, $\alpha = 15$ deg.

Fig. 7 Vortex trajectories.

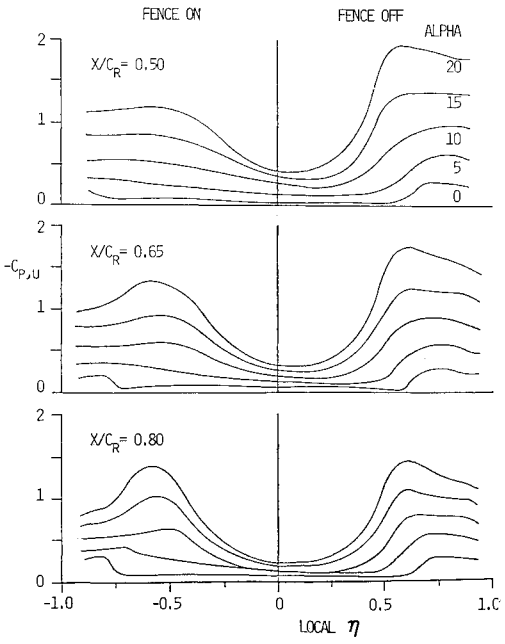

Fig. 8 Upper surface pressure distribution, asymmetric fence.

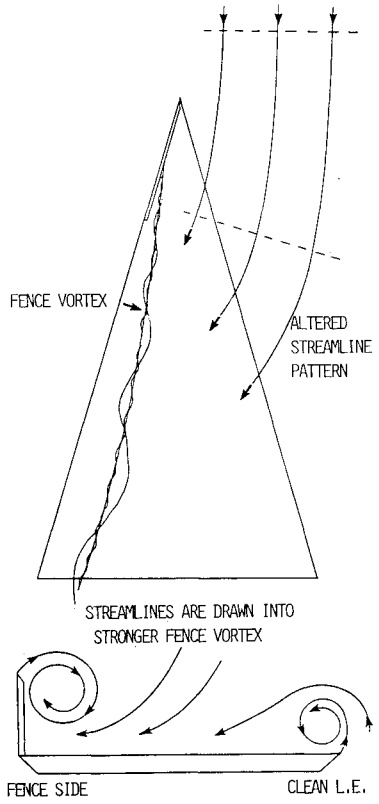

Fig. 9 Asymmetric fence effect on flowfield.

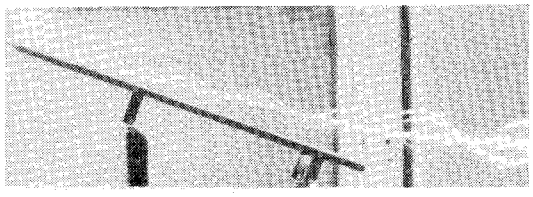

a) Planar, $\alpha = 20$ deg.

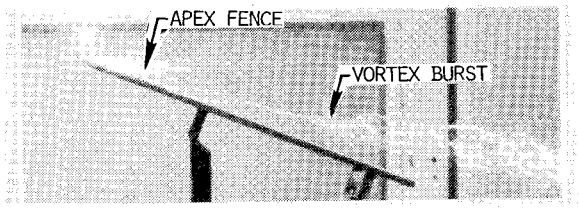

b) Asymmetric fence, clean leading-edge side ($\alpha = 20$ deg).

Fig. 10 Vortex breakdown.

the greater spanwise deflection of the oil streaks. This correlates with the higher induced suction peaks already noted in the pressure data. Intense vortex footprints were also present on the wing surface between the fences (unfortunately, a region obscured in the photographs). Therefore it is reasonable to expect that the apex area will be subject to intense suction and thus generate a high local normal force in the fence region.

A comparison of helium bubble visualization of the symmetric fence arrangement and the planar wing at $\alpha = 15$ deg is presented in Fig. 7. These side views clearly show the fence-generated vortex core trailing at a nearly constant height above the wing, while the leading-edge vortex of the planar wing is continuously rising away from the surface in the streamwise direction.

Further documentation of helium bubble flow visualization can be found in Ref. 5.

Asymmetric Apex Fences

The upper-surface pressures across the wing span, with the fence installed only on the left side, are presented in Fig. 8. Since only the right semispan was pressure-tapped, two separate tests were conducted with the fence being shifted from one side to the other between tests in order to construct the "full-span" pressure distributions depicted in Fig. 8. As expected, these distributions are asymmetrical, with the suction peaks on the fence side occurring more inboard than on the opposite side. More significantly, the suction peaks on the clean leading-edge side are considerably magnified in comparison with the planar wing. A suggested cause is the sidewash induced toward the fence, which will reduce the effective sweep (as depicted in Fig. 9) and, therefore, increase the strength of the vortex of the clean leading edge.

A noteworthy feature supporting this idea emerges from the helium bubble tests at $\alpha = 20$ deg. Two photographs were obtained with the bubble wand being moved from the clean leading edge to the opposite fence-side leading edge. From Fig. 10, it is seen that vortex breakdown occurs on the clean leading edge of the asymmetric case, while the planar case still generates stable vortices. A reduction in effective leading-edge sweep destabilizes the vortex, thus causing breakdown at a lower angle of attack.

Another observation involves the vortex trajectory. The vortex of the clean leading edge trails closer to the surface than that generated by the planar wing, while the fence vortex of the asymmetric case trails higher than that of the symmetrically deployed case.[5] This effect, along with the supposition shown in Fig. 9, results in the pressure distributions that show the suction increases on the clean side as compared to the fence side (compare Figs. 3 and 8). This result was not expected and displays the significance of the vortices interacting with one another. The oil flow patterns of Fig. 11 also show the unequal vortices generated by this asymmetrical configuration.

The lateral-directional characteristics due to the deployment of a single fence would depend on the side force acting on the fence itself and the fence vortex effects induced on the downstream surfaces. To determine those effects, balance tests would be necessary.

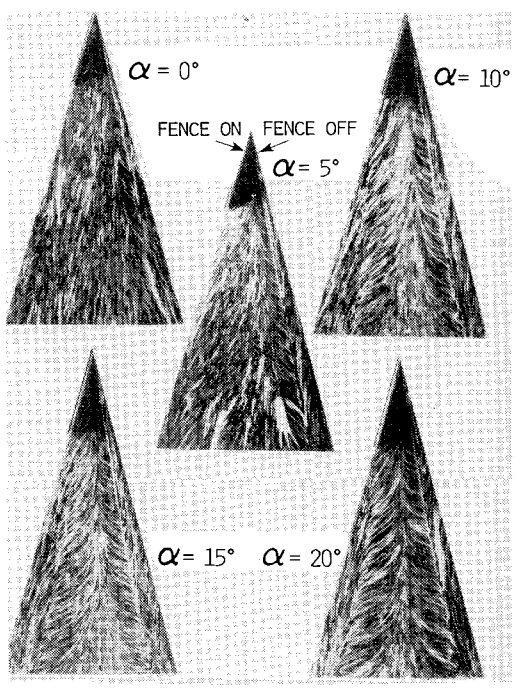

Fig. 11 Surface oil flow visualization asymmetric fence.

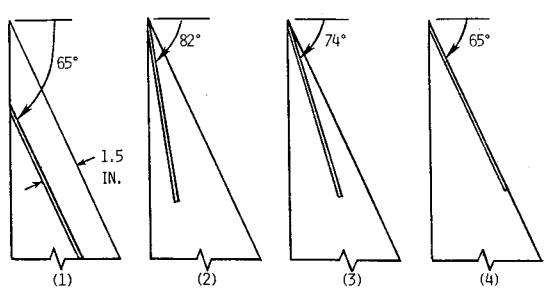

Fig. 12 Apex fence positions.

Model 2

Cases presented in this section consist of the delta and cropped-delta fences, each tested at three of the four positions on the apex region of the wing (Fig. 12). Further documentation on model 2 tests can be found in Refs. 6 and 7.

Flow Patterns

The delta fence was tested at the 65 and 74 deg sweep positions as well as the location parallel to, but displaced from, the leading edge. Helium bubble photos for these cases are presented in Fig. 13. For the 65 deg case, the fence vortex bends outward toward the leading-edge vortex and subsequently experiences breakdown by $\alpha = 20$ deg. The fence was then moved to the 74 deg position in an attempt to limit the fence/leading-edge vortex interaction. However, this configuration did not alleviate the adverse interaction. The fence position parallel to, but displaced from, the leading edge was then chosen as another attempt to limit the interaction by increasing the separation between the two vortices. Again, the vortices merge and experience breakdown at high angles of attack. However, a benefit gained from this position, as well as from that at 74 deg, is that the leading-edge vortex acts on the

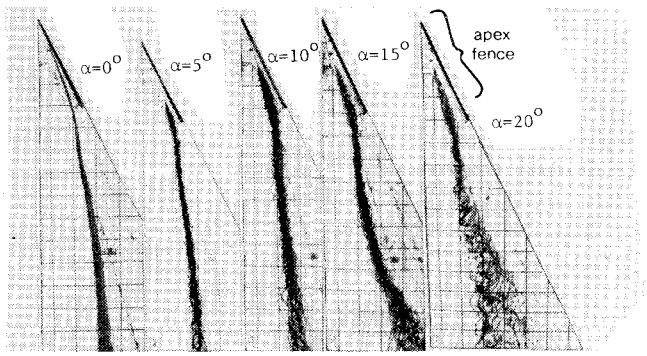

a) $\Lambda_f = 65$ deg fence position.

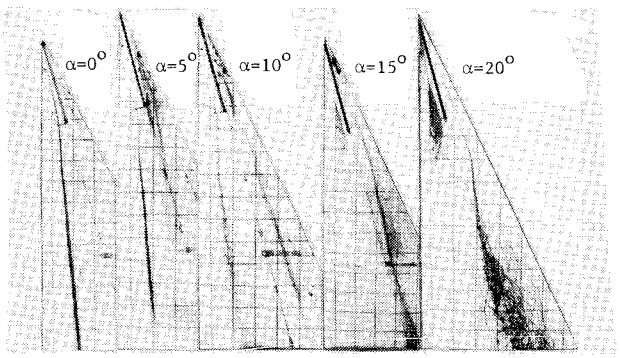

b) $\Lambda_f = 74$ deg fence position.

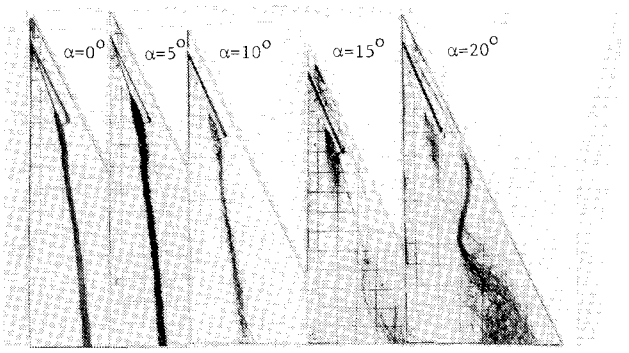

c) Parallel fence position.

Fig. 13 Delta fence flow patterns.

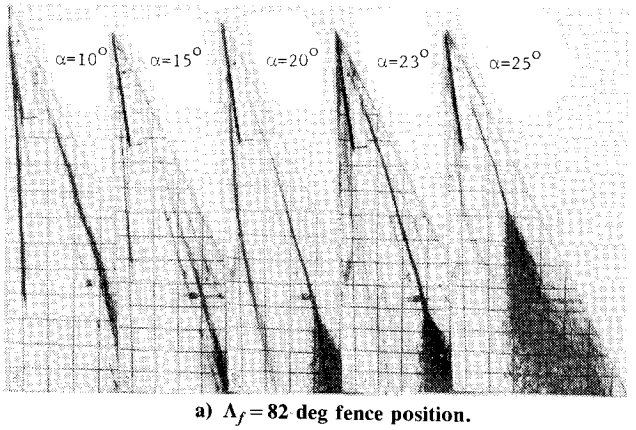

a) $\Lambda_f = 82$ deg fence position.

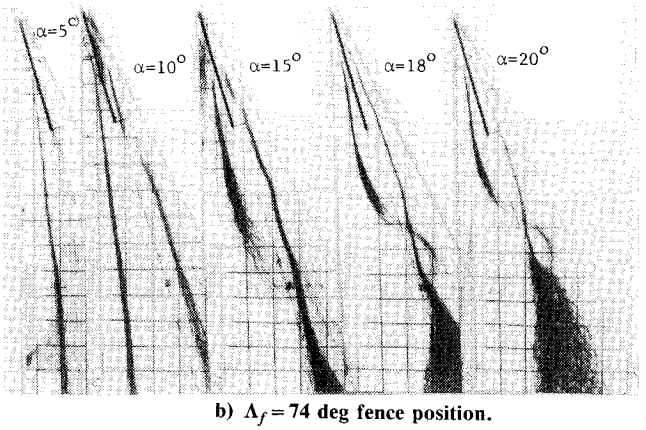

b) $\Lambda_f = 74$ deg fence position.

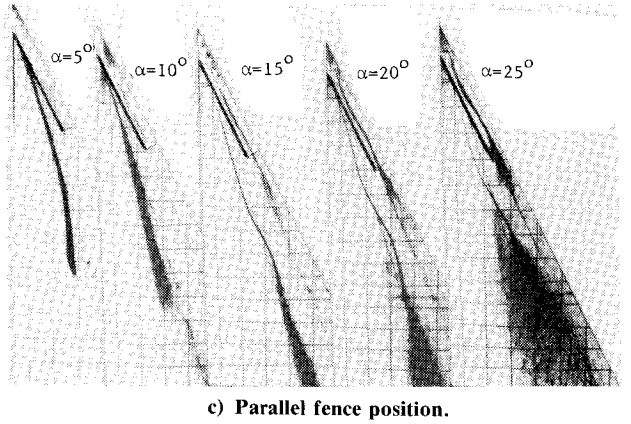

c) Parallel fence position.

Fig. 14 Cropped delta fence flow patterns.

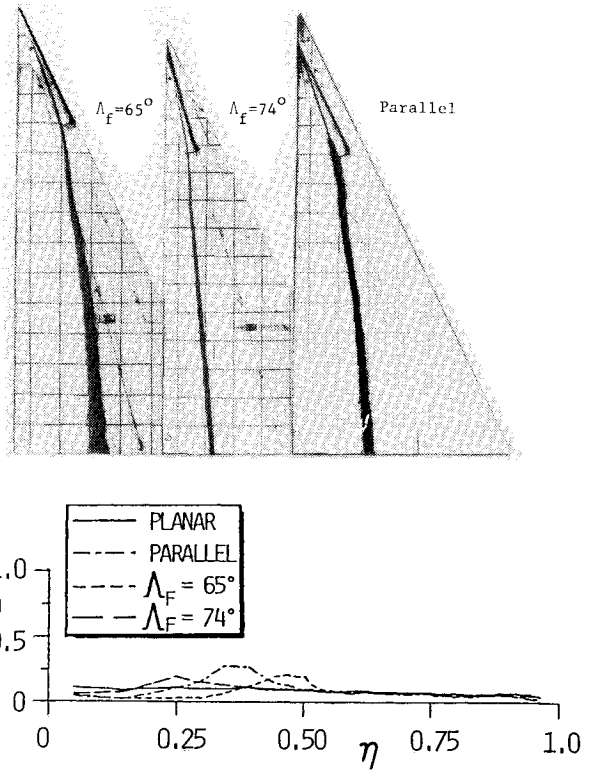

Fig. 15 Delta flap cases, $\alpha = 0$ deg.

Table 1 Local average pressure coefficients, $-\overline{C}_{p,u}$

Configuration	Angle of attack, deg 0	10	20
Planar	0.087	0.421	0.785
Delta flap			
$\Lambda_f = 65$ deg	0.070	0.427	0.803
$\Lambda_f = 74$ deg	0.090	0.467	0.780
Parallel	0.091	0.487	0.772
Cropped delta flap			
$\Lambda_f = 74$ deg	NA[a]	0.470	0.722
$\Lambda_f = 82$ deg	NA	0.452	0.812
Parallel	NA	0.471	0.719

[a]Not applicable for this case.

outside face of the fence, thus providing a thrust component to reduce drag or a side force component for potential flight path control.

The cropped-delta fence was tested at the parallel, 74, and 82 deg sweep positions as depicted in Fig. 14. As with the delta fence, the cropped-delta fence at the 74 deg and parallel positions clearly display vortex merging followed by breakdown at high angles of attack. With the fence sweep at 82 deg, the fence itself is at an incidence of 8 deg relative to the free-stream (consider the fence as an isolated surface). This is of particular importance in this case as a highly swept shape will not generate significant vortex strength at such a low incidence angle. Although the fence sweep angle determines the geometric incidence of the fence, it should be noted that, at moderate-to-high angles of attack of the wing, the leading-edge vortex induces an upwash on the fence. This effectively allows a fence incidence greater than 8 deg and, thus, a stronger fence vortex than expected. This configuration succeeded in separating the fence/leading-edge vortices through $\alpha = 20$ deg, at which point the leading-edge vortex bursts, as in the planar case, while the fence vortex remains intact past the trailing edge of the wing.

Configuration Comparisons

Flow patterns and pressure distributions are presented here for comparison. Data for the delta fence are given in Figs. 15–17 for angles of attack of 0, 10, and 20 deg, respectively. While qualitatively similar at $\alpha = 0$ deg, there is a noticeable difference in the suction peak location as well as the local upper-surface pressure distribution. Table 1 presents the calculated local $-\overline{C}_{p,u}$ for all fence positions at $\alpha = 0$, 10, and 20 deg. When compared with the planar wing at $\alpha = 0$ deg, the 65 deg fence position shows a 19.5% decrease in $-\overline{C}_{p,u}$ while the 74 deg and parallel positions show a net increase of 3.4 and 4.6%, respectively. At this angle of attack, the leading-edge

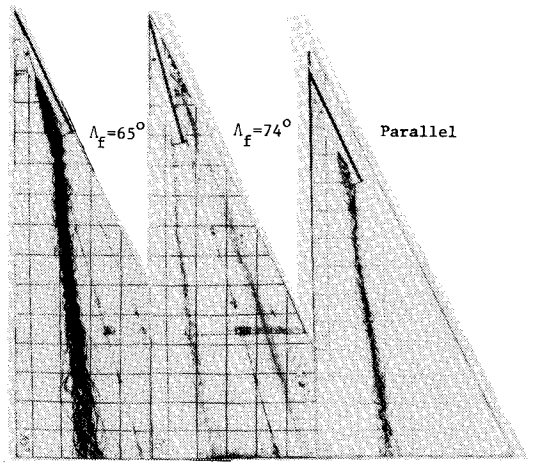

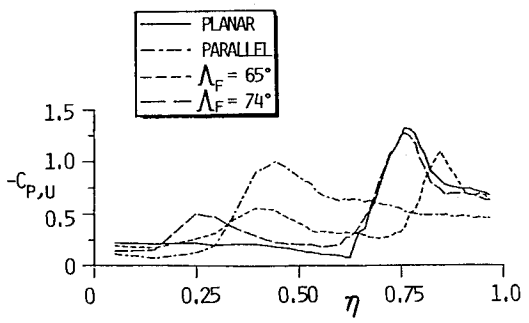

Fig. 16 Delta flap cases, $\alpha = 10$ deg.

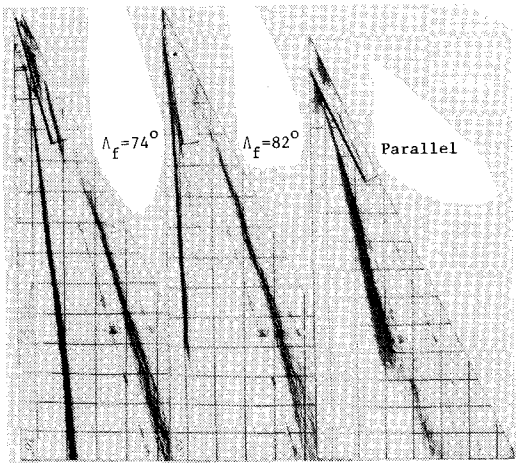

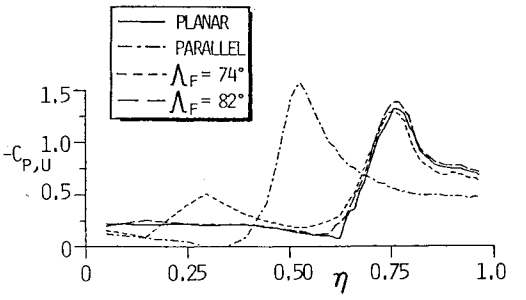

Fig. 18 Cropped flap cases, $\alpha = 10$ deg.

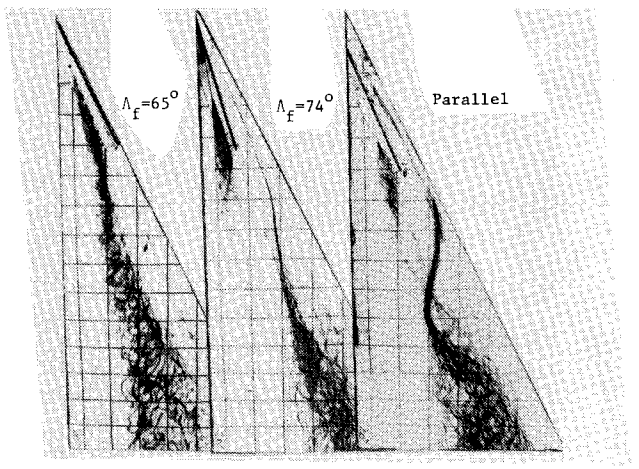

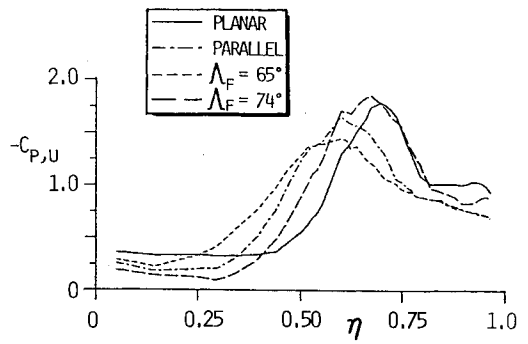

Fig. 17 Delta flap cases, $\alpha = 20$ deg.

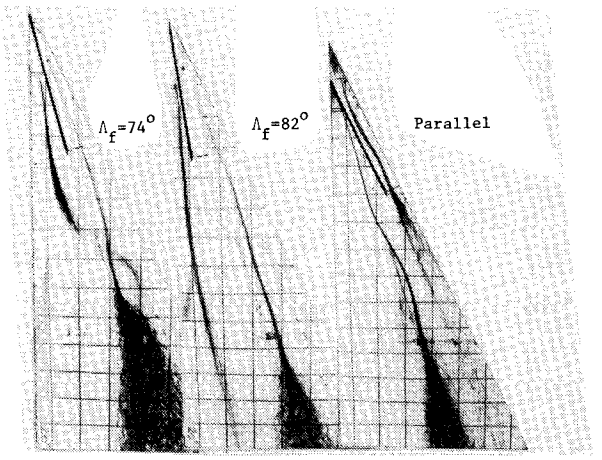

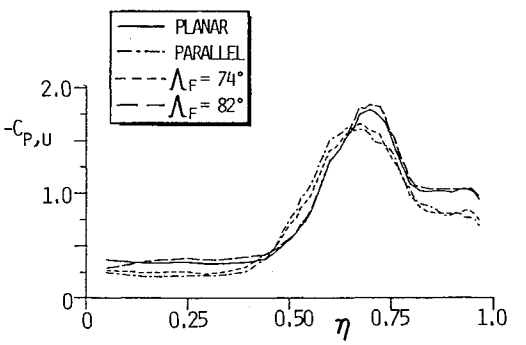

Fig. 19 Cropped flap cases, $\alpha = 20$ deg.

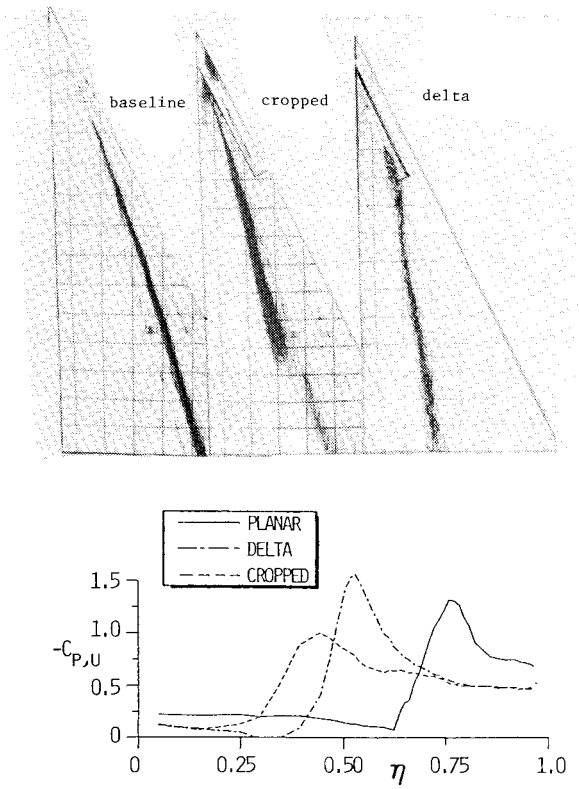

Fig. 20 Parallel fence comparison, $\alpha = 10$ deg.

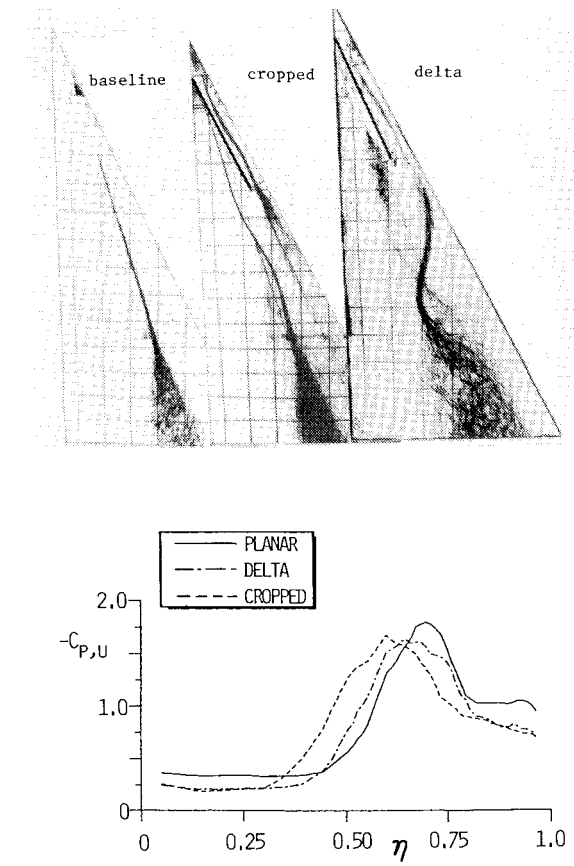

Fig. 21 Parallel fence comparison, $\alpha = 20$ deg.

vortex is not present, so the fence vortex dominates the flowfield over the wing. The downwash on the inboard section of the wing due to the counterclockwise rotation of the fence vortex acts over a larger portion of the semispan for the 65 deg case, thus causing the net $-\overline{C_{p,u}}$ to be much lower than that for the cases where the fence is positioned further inboard. At an angle of attack of 10 deg, the leading-edge vortex has achieved significant strength, producing the second suction peak closer to the leading edge. Here, $-\overline{C_{p,u}}$ increases for each of the fence positions. For the parallel case, the vortex pair has merged upstream of the tap station, resulting in a single, strong suction peak that produces a 15.7% increase in $-\overline{C_{p,u}}$ over the planar wing. At $\alpha = 20$ deg, this merging occurs for each of the fence positions and vortex bursting becomes evident. In this case, only the 65 deg fence location results in an increase in local $-\overline{C_{p,u}}$.

Comparisons of the parallel, 74, and 82 deg locations of the cropped-delta fence are presented in Figs. 18 and 19. At $\alpha = 10$ deg, all fence positions produce an increase in $-\overline{C_{p,u}}$ with the parallel and 74 deg cases showing an approximate increase of 12% over the planar wing. Figure 19 displays the advantage of the 82 deg fence position in that the fence and leading-edge vortices have yet to interact, yielding increased suction levels due to the postponement of the merge/burst point phenomenon.

A more direct indication of the effect of fence shape is given in Figs. 20 and 21 where the fence is in the parallel position. At $\alpha = 10$ deg (Fig. 20), the effect of simply "cropping" the delta fence is seen as a significant change in the strength and position of the suction peak. As the angle of attack is increased to 20 deg, the cropped fence tends to delay the merging of the fence and leading-edge vortices. Also of particular interest is the difference in the vortex patterns near the apex region where, for the delta fence case, the fence vortex experiences an early burst.

Since the preparation of this paper, a force and moment study[8] has been conducted, confirming many of the trends discussed here.

Conclusions

The apex fence was found to have significant effects on the flowfield of two different delta planforms due to fence-generated vortices. Upper-surface suction levels were enhanced and, when averaged across the local semispan, amounted to a 10% increase over the planar wing for the angle of attack range of this test. Indications are that even higher suction levels may occur in the apex region between the fences, producing a nose-up pitching moment for longitudinal trimming (i.e., when trailing-edge flaps are deployed). Asymmetrically deployed fences should also have potential for lateral-directional control at high angles of attack.

The geometry and position of the fence were also shown to have a major effect in the avoidance of the merging of the leading-edge vortex with the fence vortex that caused premature bursting of the vortex pair with a subsequent degradation in the upper surface suction level.

Acknowledgments

This investigation was supported by NASA Langley Research Center under Cooperative Agreement NCC1-46. The authors very much appreciate the assistance of the following people: Dr. D.M. Rao for initiating the project and providing technical insight, Mr. W.E. Schoonover Jr. for serving as Langley technical monitor, and Dr. F.R. DeJarnette of North Carolina State University for serving as university project monitor.

References

[1]Rao, D.M., "Vortical Flow Management for Improved Configuration Aerodynamics-Recent Experiences," presented at AGARD

Symposium on Aerodynamics of Vortical Type Flows in Three Dimensions, Paper 30, 1983.

[2]Rao, D.M., "Upper Vortex Flap—A Versatile Surface for Highly Swept Wings," presented at ICAS 13th Congress, paper 82-6.7.1, 1982.

[3]Buter, T.A., "Experimental and Computational Investigation of an Apex Flap Concept on a 74-Degree Delta Wing," M.S. Thesis, North Carolina State University, Raleigh, Feb. 1983.

[4]Rao, D.M. and T.A. Buter, "Experimental and Computational Studies of a Delta Wing Apex-Flap," AIAA Paper 83-1815, July 1983.

[5]Wahls, R.A. and R.J. Vess, "An Exploratory Study of Apex Fence Flaps on a 74-Degree Delta Wing," NASA CR-172463, May 1985.

[6]Wahls, R.A., R.J. Vess, and C.A. Moskovitz, "An Experimental Investigation of Apex Fence Flaps on Delta Wings," AIAA Paper 85-4055, Oct. 1985.

[7]Moskovitz, C.A., "An Experimental Investigation of Optimizing Vortex Fence Flaps," NASA CR to be published.

[8]Hoffler, K.D., D.M. Rao, and M.C. Frassenelli, "Basic Studies on Delta Wing Flow Modifications by Means of Apex Fences," NASA CP-2416, Oct. 1985.